532.542:532.527

Paper No. 214-4

Flow in an Axially Rotating Pipe

(A calculation of flow in the saturated region)*

By Koji KIKUYAMA**, Mitsukiyo MURAKAMI***,
Kenji NISHIBORI**** and Kazuhiko MAEDA*****

If a flow enters an axially rotating pipe, it receives a tangential component of velocity from the moving wall, and the flow pattern and hydraulic loss suffer a change according to the ratio of the rotational speed to the through flow velocity.

A flow laminarization is set up by an increase in the rotational speed of the pipe if the flow in the pipe is initially turbulent, and a flow destabilization is brought conversely about if the flow is initially laminar.

Velocity distributions and friction coefficient in the fully developed region of the pipe were calculated by using a modified mixing length theory, and the results were compared with those by the experiments.

Key words: Turbulence, Rotating Pipe, Mixing Length, Velocity Distribution, Friction Factor, Laminarization

1. Introduction

When a flow enters an axially rotating pipe, a swirling component of velocity is given to the flow by the moving wall and it causes large changes both in the time-mean velocity profiles and the turbulent structure of the flow, resulting in a change in the flow resistance.

The effects of the pipe rotation on the hydraulic loss have been investigated experimentally by many researchers (1)∿(3). The present authors (4) also measured the time-mean velocity components and hydraulic losses in axially rotating pipes when a fully developed turbulent flow was introduced into the pipe. The pipe rotation was found to suppress the turbulence in the flow, and also to reduce the hydraulic loss. The axial velocity in this case approaches a laminar flow type (parabolic) with an increase in the rotational speed of the pipe. The suppression of the turbulence due to the pipe rotation was also investigated in the boundary layer flow inside the rotating pipes when an undeveloped flow with a rectangular axial velocity distribution was introduced into them (5).

Yamada and Imao (6) measured the velocity profiles and hydraulic loss in a saturated downstream region of a rotating pipe when a fully turbulent flow was introduced in the pipe, and found the same kind of flow change as in the authors study. When the inlet flow is laminar, however, the pipe rotation gives the opposite effects: the hydraulic loss is increased and the axial velocity profile tends to be a turbulent flow type.

The changes of the flow patterns in a rotating system in case of the turbulent flow entrance were calculated by Koosinlin, et al. (7) using a modified mixing length theory, Aguilar and Pierce (8) using an eddy viscosity model, and Launder, et al. (9) using a two-equation model of turbulence. These calculations are those for the boundary layer flow developing not inside a rotating cylinder but outside a rotating body.

This paper gives the results of calculations of velocity distribution and hydraulic loss in an axially rotating pipe in a region far downstream from its inlet section, where the effects of the rotation on the flow are supposed to be saturated. The calculation was performed, for the turbulent inlet condition, by use of a relationship between the mixing length and the Richardson number proposed by Bradshaw (10), and the results were confirmed by experiments. For a laminar flow entrance, the calculation was reasonably modified and gave satisfactory results.

2. Nomenclature

a : pipe radius $=d/2$
d : pipe diameter

* Received 8th May, 1981.

** Associate Professor, Department of Mechanical Engineering, Nagoya University, Furocho, Chikusaku, Nagoya, Japan.
*** Professor, Department of Mechanical Engineering, Nagoya University.
**** Research Associate, Department of Mechanical Engineering, Nagoya University.
***** Engineer, Mitsubishi Motor Company LTD, Hashime-cho, Okazaki, Aichi.

h_l : loss of head between two sections along rotating pipe
l : mixing length in rotating pipe
l_0 : mixing length in stationary pipe
N : rotation rate $=R_{ew}/R_e$
p : static pressure
r : radial distance
r' : dimensionless value of r $=r/a$
R_e : Reynolds number based on mean axial flow velocity $=U_m d/\nu$
R_{ew} : rotational Reynolds number based on peripheral speed of rotating pipe $=V_0 d/\nu$
$R_{e\tau}$: Reynolds number based on friction velocity $=U_\tau a/\nu$
R_i : Richardson number defined by Eq. (16)
U : time-mean axial velocity
U' : dimensionless value of U $=U/U_\tau$
U_c : time-mean axial velocity at pipe center
U_m : mean value of U over a pipe section
U_τ : friction velocity $=\sqrt{\tau_{rx0}/\rho}$
V : time-mean tangential velocity
V_0 : peripheral speed of rotating pipe
W : time-mean radial velocity
u, v, w : fluctuation velocity components in x, θ, and r directions, respectively
x : axial distance from rotating pipe inlet
z : radial distance from pipe wall $=a-r$
Z^+ : dimensionless value of z $=U_\tau z/\nu$
β : parameter in Eq. (15)
κ : Kármán constant
λ : coefficient of friction loss of rotating pipe
λ_0 : coefficient of friction loss of stationary pipe
τ_{rx} : shear stress in x direction
τ_{rx0} : value of τ_{rx} at pipe wall
$\tau_{r\theta}$: shear stress in θ direction
θ : coordinate in tangential direction
ν : kinematic viscosity
ρ : density

3. Theory

3.1 Governing equations of motion

When a flow from a stationary pipe is introduced into an axially rotating pipe, a saturated state of flow can be attained in the sections far downstream from the pipe inlet and in those sections the time-mean velocity profile remains unchanged toward downstream.

Using a cylindrical coordinate system as illustrated in Fig. 1, the equations of motion in the pipe can be written as follows:

$$-\frac{\partial p}{\partial x}=\frac{1}{r}\frac{\partial(r\tau_{rx})}{\partial r} \quad \cdots\cdots(1)$$

$$\frac{1}{r^2}\frac{\partial(r^2\tau_{r\theta})}{\partial r}=0 \quad \cdots\cdots(2)$$

$$-\frac{\rho V^2}{r}=\frac{1}{r}\frac{\partial(r\sigma_r)}{\partial r}-\frac{\sigma_\theta}{r} \quad \cdots\cdots(3)$$

where

$$\tau_{rx}=-\mu\partial U/\partial r-\rho\overline{uw} \quad \cdots\cdots(4)$$

$$\tau_{r\theta}=-\mu r\partial/\partial r(V/r)-\rho\overline{vw} \quad \cdots\cdots(5)$$

$$\sigma_r=-p-2\mu\partial W/\partial r-\rho\overline{w^2} \quad \cdots\cdots(6)$$

$$\sigma_\theta=-p-\rho\overline{v^2} \quad \cdots\cdots(7)$$

In the above equations (U,V,W) and (u,v,w) are the time-mean and turbulent components of velocities in x, θ, and r directions, respectively. Integration of Eq. (1) gives

$$\tau_{rx}=-(\partial p/\partial x)(r/2) \quad \cdots\cdots(8)$$

Introducing the friction coefficient of the pipe, λ, the pressure gradient along the pipe can be expressed by the following equation,

$$-\partial p/\partial x=\rho\lambda U_m^2/4a \quad \cdots\cdots(9)$$

From Eqs. (8) and (9), $(\partial p/\partial x)$ can be eliminated and we have

$$\tau_{rx}/\rho=(\lambda/8)(r/a)U_m^2 \quad \cdots\cdots(10)$$

On the pipe wall τ_{rx0} becomes

$$\tau_{rx0}/\rho=(\lambda/8)U_m^2 \quad \cdots\cdots(11)$$

The equations (1) to (11) are also valid for a laminar state of flow, if the turbulent velocity components are made zero, namely $u = v = w = 0$.

3.2 Mixing length model

3.2.1 In case of turbulent flow entrance

Using Prandtl's mixing length theory, the axial shear stress τ_{rx} in Eq. (10) can be represented as follows when the flow state is turbulent.

$$\tau_{rx}=-\mu\frac{\partial U}{\partial r}-\rho l^2\left[\left(\frac{\partial U}{\partial r}\right)^2+\left\{r\frac{\partial}{\partial r}\left(\frac{V}{r}\right)\right\}^2\right]^{1/2}\frac{\partial U}{\partial r} \quad \cdots\cdots(12)$$

where l is the mixing length. Substitution of Eq. (10) into Eq. (12) yields

$$l^2\left[\left(\frac{\partial U}{\partial r}\right)^2+\left\{r\frac{\partial}{\partial r}\left(\frac{V}{r}\right)\right\}^2\right]^{1/2}\frac{\partial U}{\partial r}=-\frac{\lambda}{8}U_m^2\frac{r}{a}-\nu\frac{\partial U}{\partial r} \quad \cdots\cdots(13)$$

For a fully developed turbulent pipe flow ($R_e \geqq 10^5$), the mixing length in a stationary pipe, l_0, has been expressed by the following equation.

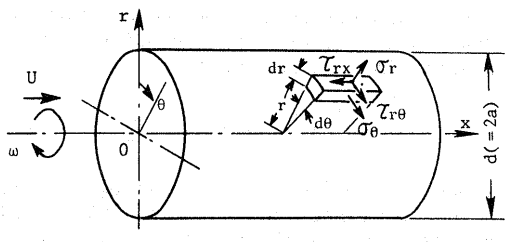

Fig. 1 Cylindrical coordinate

$$\frac{l_0}{a}=\kappa\left\{0.35-0.2\left(\frac{r}{a}\right)^2-0.15\left(\frac{r}{a}\right)^4\right\} \quad \cdots\cdots(14)$$

where κ denotes the Kármán constant, and $\kappa = 0.4$. If the flow Reynolds number is reduced under the limit, the value of the mixing length will deviate from that obtained by Eq. (14), but the expression itself may be considered to be available even in a low Reynolds number range.

In a rotating system, the mixing length l may be changed by the effect of the centrifugal force. To express the degree of turbulence suppression due to the centrifugal force, the mixing length given by Eq. (14) must be modified by using Bradshaw's formula as,

$$l/l_0=1-\beta R_i \quad \cdots\cdots(15)$$

where β is a constant, and R_i is the Richardson number defined by

$$R_i=\frac{2(V/r^2)\partial/\partial r(rV)}{(\partial U/\partial r)^2+\{r\partial/\partial r(V/r)\}^2} \quad \cdots\cdots(16)$$

In the above equations, both of R_i and mixing length are assumed to be functions of the axial and tangential components of velocities.

According to the experiments by the present authors (4) and also by Yamada and Imao (6), the profile of tangential velocity, V, in the rotating pipe does not exhibit an exact forced vortex type distribution even in the sufficiently downstream sections of $x/d \geqq 120$ if the inlet flow is turbulent. In this case a parabolic distribution as expressed by the following equation is available.

$$V/V_0=(r/a)^2 \quad \cdots\cdots(17)$$

To express the rotation rate of the pipe, a dimensionless value defined by the ratio of the peripheral speed of the pipe V_0 to the mean axial velocity of the flow U_m is introduced:

$$N=V_0/U_m \quad \cdots\cdots(18)$$

Substituting Eqs. (17) and (18) into Eq. (16), the Richardson number can be written as

$$R_i=\frac{6N^2(r/a)^2}{\{\partial(U/U_m)/\partial(r/a)\}^2+\{(r/a)N\}^2}=\frac{6N^2r'^2}{\{\partial/\partial r'(U/U_m)\}^2+r'^2N^2} \quad \cdots\cdots(19)$$

where $r'=r/a$

3.2.2 In case of laminar flow entrance

Pedley (11) analyzed the stability of a laminar flow with a rigid rotation in a rotating pipe and showed that the pipe rotation had a destabilizing effect on the flow if the axial Reynolds number Re was greater than 82.9. From the measured value of the hydraulic loss experienced in the rotating pipe, within the range of $R_e < 2300$, it is ascertained that the flow changes gradually into a turbulent state as the rotational speed of the pipe is increased (6). In order to express this destabilizing effect of the pipe rotation when a laminar flow is introduced, the second term on the right hand side of Eq. (12) must be retained. Then the mixing length l/l_0 is considered to be a function of the rotational Reynolds number R_{ew} and

$$l/l_0=f(R_{ew}) \quad \cdots\cdots(20)$$

In this case the distribution of the tangential components of velocity can be assumed to be a forced-vortex type expressed as

$$V/V_0=r/a \quad \cdots\cdots(21)$$

3.3 Relations necessary for description of velocity distribution and friction coefficient

From Eq. (11) the friction velocity U_τ can be obtained as

$$U_\tau=\sqrt{\tau_{rx0}/\rho}=\sqrt{\lambda/8}\,U_m \quad \cdots\cdots(22)$$

With use of Eq. (22), Eq. (13) can be transformed into a dimensionless form as

$$\left(\frac{l}{a}\right)^2\sqrt{1+\left(\frac{Nr'U_m/U_\tau}{dU'/dr'}\right)^2}\left(\frac{dU'}{dr'}\right)^2-\frac{1}{R_{e\tau}}\left(\frac{dU'}{dr'}\right)-r'=0 \quad \cdots\cdots(23)$$

when the inlet flow is turbulent, and

$$\left(\frac{l}{a}\right)^2\left(\frac{dU'}{dr'}\right)^2-\frac{1}{R_{e\tau}}\left(\frac{dU'}{dr'}\right)-r'=0 \quad \cdots\cdots(24)$$

when the inlet flow is laminar. In the above equations, $\partial U'/\partial r'$ is replaced by dU'/dr' and $U'=U/U_\tau$, and $R_{e\tau}$ denotes a Reynolds number based on the friction velocity as

$$R_{e\tau}=U_\tau a/\nu \quad \cdots\cdots(25)$$

Noticing that both of Eqs. (23) and (24) are quadratic in terms of (dU'/dr') and that the coefficients of each term in the equations are given by Eqs. (14)~(16) for a turbulent flow entrance and by Eq. (20) for a laminar flow entrance, the gradient of the axial velocity (dU'/dr') can be determined at any radial position. With this value the velocity U' at any radial distance is given by

$$U'=\int_1^{r'}\left(\frac{dU'}{dr'}\right)dr'=\int_0^{z'}\left(\frac{dU'}{dz'}\right)dz' \quad \cdots\cdots(26)$$

where $z'=1-r'$. Integrating Eq. (26) across pipe section, a dimensionless value of the mean axial velocity, u_m, can be estimated by the following relation as

$$u_m \equiv \frac{U_m}{U_\tau} = 2\int_0^1 r'U'dr' \quad \cdots\cdots(27)$$

and the value of Reynolds number R_e is given by

$$R_e \equiv U_m d/\nu = 2R_{e\tau}u_m \quad \cdots\cdots(28)$$

Substituting Eq. (27) into Eq. (22), the friction coefficient, λ, is given by

$$\lambda = 8/u_m{}^2 \quad \cdots\cdots(29)$$

3.4 Boundary conditions and methods of calculation

To compute the value of (dU'/dr') numerically from Eq. (23) or (24), the radius of pipe, a, is divided into one thousand equal parts. On the pipe wall ($r=a$) the mixing length, l, becomes zero and dU'/dz' (=- dU'/dr') becomes

$$dU'/dz' = (1-z')R_{e\tau} \quad \cdots\cdots(30)$$

This equation can be applied through the viscous sublayer adjacent to the pipe wall, and the dimensionless thickness of which is assumed to be the same as in the stationary pipe as

$$Z^+ \equiv U_\tau z/\nu \leqq 11.6 \quad \cdots\cdots(31)$$

When a turbulent flow enters the rotating pipe, the value of β in Eq. (15) may be taken as 0.4 and 0.5, taking account of the experimental data described later. Much more different value of β has been found in the other studies: Koosinlin and his co-workers found the result of $\beta = 5$ for their study on the external flow around a rotating cylinder, and the present authors obtained the value of $\beta = 2 \sim 3$ in the study on the boundary layer flow developing in a rotating pipe [12]. Compared with these data, the value of $\beta = 0.4 \sim 0.5$, which is available in the present study, is much smaller.

In the case when a laminar flow is introduced into the rotating pipe, l/l_0 in Eq. (20) can be assumed to be given by the following equation.

$$l/l_0 = 0.012R_{ew}{}^{0.5} \quad \cdots\cdots(32)$$

In this case the flow in the region of $Z^+ \leqq 5.0$ is assumed to remain laminar due to the presence of a viscous sublayer near the pipe wall.

For the velocity profile and the friction coefficient of the pipe, λ, calculations can be made by using an assumed value of $R_{e\tau}$ corresponding to the given values of N, R_e, and R_{ew}. Value of (dU'/dr') at any radial point can be obtained for this assumed value of $R_{e\tau}$, and with this value the axial Reynolds number can be calculated by use of Eqs. (27) and (28). The value of R_e calculated by this method may deviate from that of R_e given initially. If the differnce between these two values, namely ε, exceeds the value of $R_e/1000$, the above process of calculation is repeated with another corrected value of $R_{e\tau}$ until ε falls within the range $|\varepsilon| \leqq R_e/1000$.

4. Apparatus and method of experiment

In order to confirm the calculated results, experiments were carried out with hydraulically smooth pipes of two different diameters of d = 20.0 mm and 5.0 mm. Figure 2 shows a schematic outline of the experimental apparatus. Water delivered from an overflow tank was led to a rectifying tank, upstream stationary pipe (l_1 = 100d), a rotating pipe and a downstream stationary pipe, successively. The rotating pipe was driven by a variable speed motor.

Static pressure on the rotating pipe wall was introduced into a stationary system through the mechanical seals. Figure 3 shows the location of sections at which the hydraulic loss of the rotating pipes was measured. To exclude the effect of the inlet region on the pressure measurement, the pressure tappings were provided at the sections A(x = 145d) and C(x = 175d) on the pipe 1(d = 20.0 mm), and A(x = 286d) and C(x = 369d) on the pipe 2(d = 5.0 mm), respectively. With use of hydraulic loss of head, h_l, obtained from the static pressure difference between the two sections on each pipe, the friction coefficient, λ, can be evaluated by

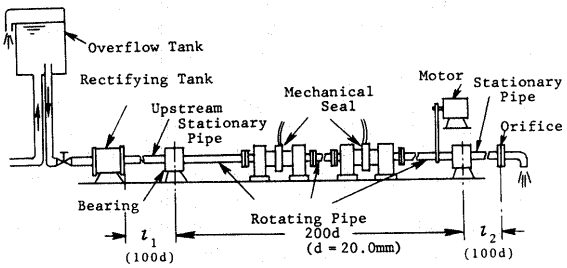

Fig. 2 Schematic of experimental apparatus

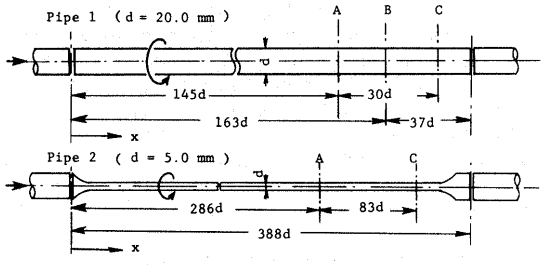

Fig. 3 Detailed dimensions of rotating pipes and measuring sections

$$\lambda = h_l / \{(l/d)(U_m^2/2g)\} \quad \cdots\cdots(33)$$

Employing a larger diameter pipe of d = 20.0 mm, the time-mean velocity components at the section $x = 163d$ were measured by a laser doppler velocimeter. The measuring section was replaced by a lucite tube through which the laser beams could pass, and maximum 50 ppm of milk was added as a tracer.

The axial Reynolds number R_e and the rotational Reynolds number R_{ew} were changed over the ranges of $500 \leqq R_e \leqq 2 \times 10^4$ and $0 \leqq R_{ew} \leqq 3.5 \times 10^4$, respectively.

5. Comparison between calculations and experiments

5.1 In case of turbulent flow entrance

5.1.1 Velocity distributions

The calculated mean velocity profiles for the axial component U and the tangential velocity component V assumed by Eq. (17) are shown for $R_e = 10^4$, 2×10^4, and 5×10^4 in Figs. 4(a), (b), and (c), respectively, in which the experimental results for the same Reynolds numbers are also plotted for comparison. In this calculation the mixing length, l, is determined from Eq. (15) with $\beta = 0.4$. The results calculated with $\beta = 0.5$ are also plotted in the same figures for reference. The thickness of the viscous sublayer in the calculations is taken to be $0 \leqq Z^+ \leqq 11.6$. When $R_e = 10^4$ as indicated in Fig. 4(a), the calculated profiles of the axial velocity are in close agreement with the experiments for all of the rotation rates within the range of $0 \leqq N \leqq 3$. An examination of the velocity profiles U/U_m shows that they approach gradually a parabolic shape with an increase in N, and correspondingly, the effect of turbulence suppression due to the pipe rotation becomes remarkable. When $R_e = 2 \times 10^4$ (Fig. 4(b)), the calculated velocity curves with $\beta = 0.4$ (solid lines) have a little lower values than the measured curves in the central region of the pipe, and the difference increases by a slight amount as N is increased. The axial velocity profiles calculated with $\beta = 0.5$ are also shown by the broken lines, the coincidence being better than the case with $\beta = 0.4$. When $R_e = 5 \times 10^4$ (Fig. 4(c)), being a Reynolds number higher than the above, the calculated profiles with the values of $\beta = 0.4$ and 0.5 agree fairly well with the experimental data obtained by Yamada et al., when $N = 1.0$. The validity of the velocity profile assumption for the tangential component by Eq. (17) may be confirmed well in Figs. 4(a), (b), and (c).

The dimensionless values of the maximum axial velocity, U_c/U_m, are plotted against N in Fig. 5. The values of U_c/U_m are seen to increase linearly with an increase in N within the range of $N > 1$, and the agreement between the caluculated and measured values is almost satisfactory ($\beta = 0.4$). Though the calculated value of U_c/U_m decreases as R_e increases, the experimental data remain almost unchanged for different Reynolds numbers within the range $10^4 \leqq R_e \leqq 10^5$.

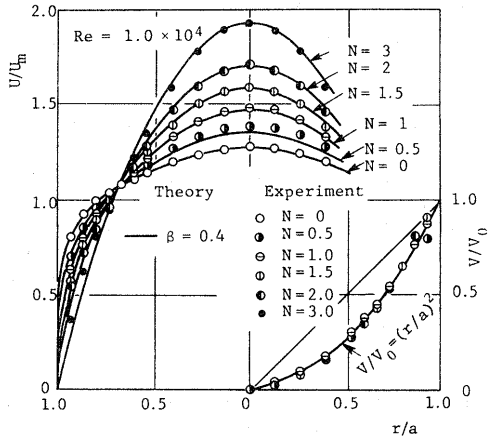

(a) $R_e = 10^4$

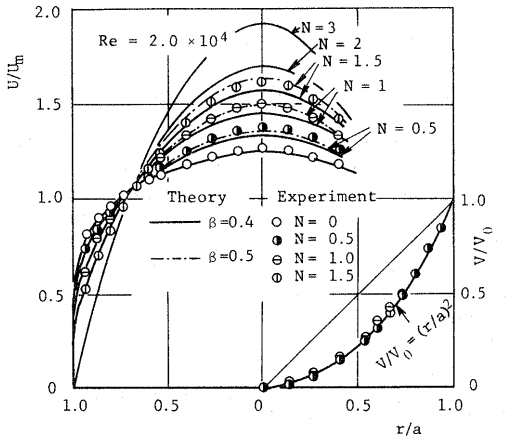

(b) $R_e = 2 \times 10^4$

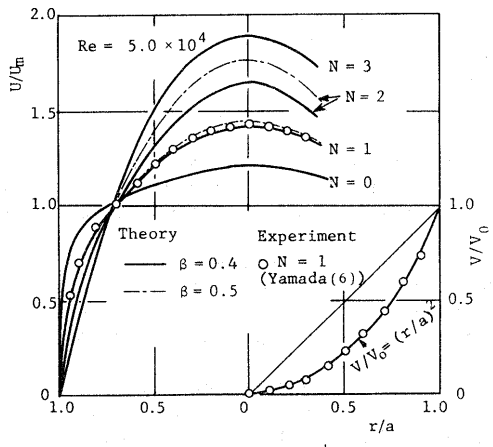

(c) $R_e = 5 \times 10^4$

Fig. 4 Velocity distributions for turbulent flow entrance

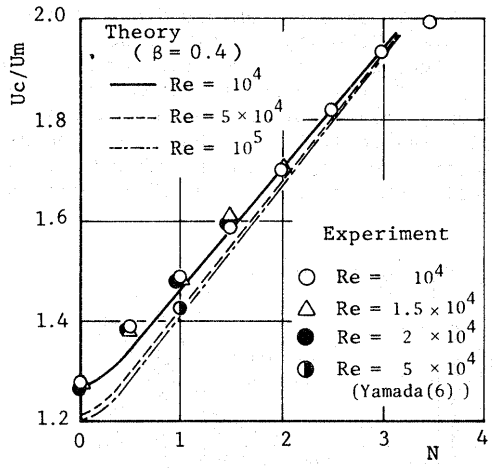

Fig. 5 Relationship between U_c/U_m and N

When N exceeds about 3.5, the value of U_c/U_m may be taken to be constant i.e. 2, and the distribution of the axial velocities substantially displays a laminar flow pattern.

5.1.2 Friction coefficient

Figure 6 shows the relationship between the friction coefficient λ, and the axial Reynolds number R_e. Solid and broken lines denote the calculated results for β = 0.4 and 0.5, respectively. The value of λ calculated with β = 0.4 exhibits a little smaller value than that with β = 0.5. In this figure the measured values of λ are also plotted for various values of N. It may be found that the calculations of velocity profiles and friction coefficient yield fairly reasonable results, if a value of β in Eq. (15) is selected between 0.4 and 0.5.

The relationship between the friction coefficient λ and the rotation rate N is shown in Fig. 7, in which λ_0 is the friction coefficient of a stationary pipe. The values of λ/λ_0 decrease with an increase in N, and this tendency becomes remarkable for larger values of R_e. The data by the other researchers also show a satisfactory agreement with one another.

5.1.3 Richardson number and mixing length

The Richardson number R_i is evaluated from Eq. (19) when $R_e = 10^4$, and its distributions across the pipe section are shown in Fig. 8. As the existence of the viscous sublayer near the pipe wall is assumed, the gradient of the axial velocity is given by the relationship $dU'/dr' = -R_{e\tau}r'$ and the Richardson number R_i in this region remains constant and,

$$R_i = \frac{6N^2}{(2R_{e\tau}^2/R_e)^2+N^2}$$

On the other hand it tends to be zero at the pipe center. The value of R_i increases with an increase of N, and the curves of R_i are flattened over the greater part of the section.

Figures 9(a) and (b) show the distributions of l/a calculated by Eqs. (14) and (15) across the section. The values of l/a are taken to be zero in the region $Z^+ \leqq 11.6$. The experimental values of l/a are those which are obtained from the relation of Eq. (13) using the measured values of the velocity gradient dU/dr and the friction

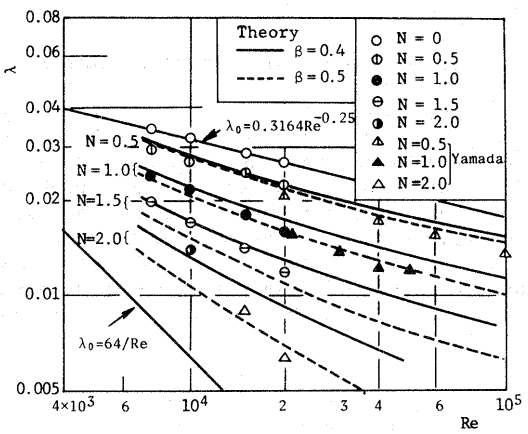

Fig. 6 Friction coefficient of rotating pipe for turbulent flow entrance

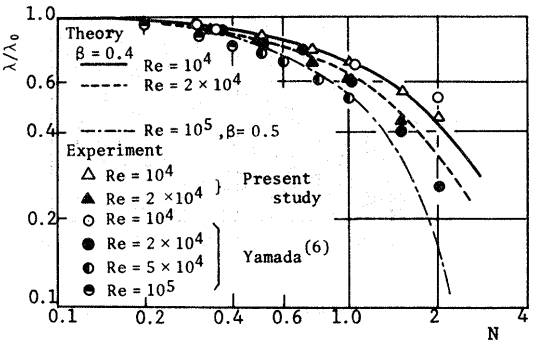

Fig. 7 Relationship between λ/λ_0 and N

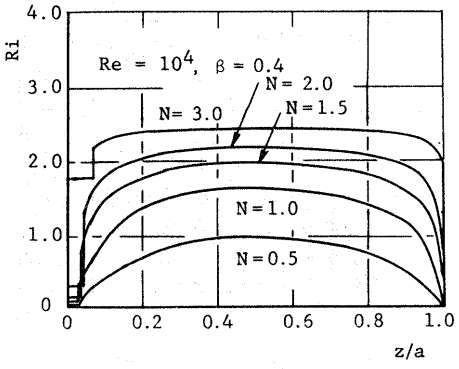

Fig. 8 Distributions of Richardson numbers

coefficient λ. When $R_e = 10^4$(Fig. 9(a)), the agreement between the calculated(β = 0.4) and measured values is sufficient except for the case when $N = 0.5$. The curves of l/a shift downward as N is increased, showing a greater suppression of turbulence for a larger value of N. A large reduction of l/a for $N = 3$ corresponds to a flow relaminarization inside the rotating pipe and the value of U_c/U_m becomes approxiamtely 1.9 as shown in Fig. 5. In Fig. 9(b) the calculated results for $\beta = 0.4$ and 0.5 are plotted when $R_e = 2 \times 10^4$. The agreement with the experiments is better for $\beta = 0.5$ than for $\beta = 0.4$.

5.1.4 Logarithmic velocity distribution

The wall law in the velocity distributions is checked in Fig. 10, where the calculated and experimental results for different R_e and N are plotted together. The agreement in the both data is fairly good except for the case of N = 1.0. As is seen in this figure, the universality of the relationship between U/U_τ and Z^+ can be secured if N remains constant.

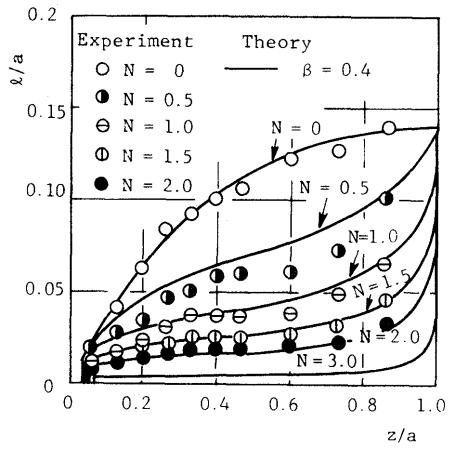

(a) $R_e = 10^4$

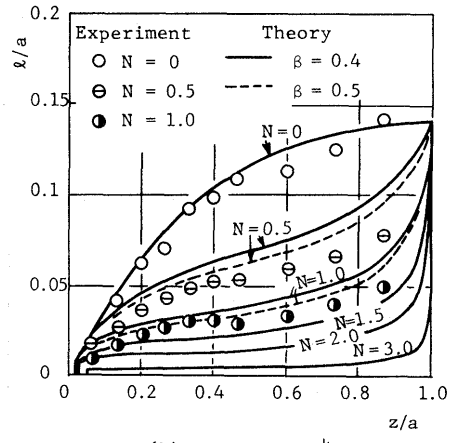

(b) $R_e = 2 \times 10^4$

Fig. 9 Distributions of l/a

5.2 In case of laminar flow entrance

5.2.1 Velocity distributions

Figures 11(a) and (b) exhibit the effect of the pipe rotation on the velocity distributions when R_e = 600 and 1000, respectively. When a laminar condition of flow is introduced into an axially rotating pipe, the flow will be

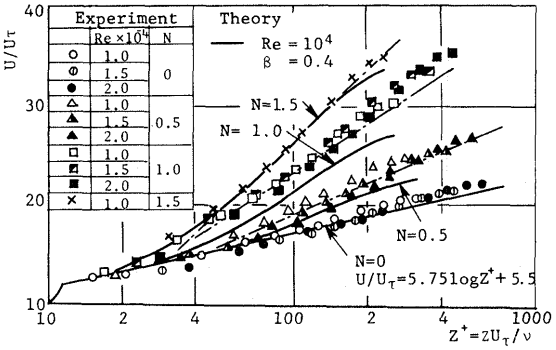

Fig. 10 Logarithmic velocity distribution

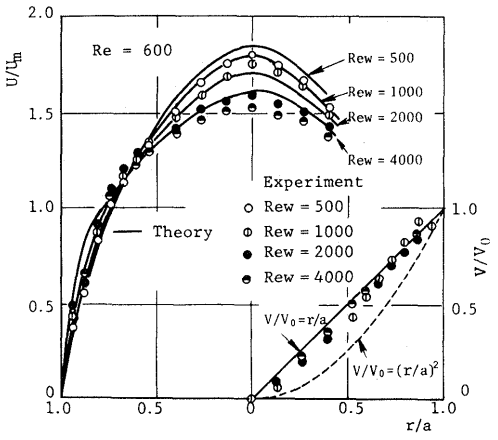

(a) $R_e = 600$

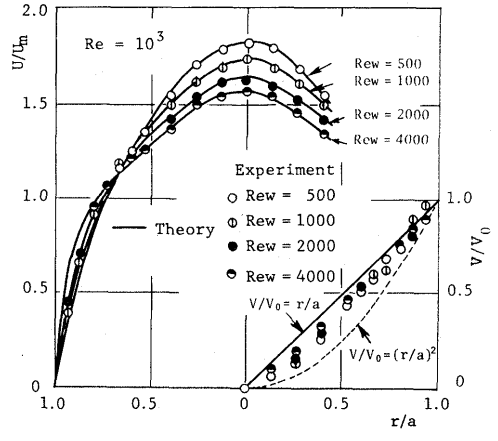

(b) $R_e = 10^3$

Fig. 11 Velocity distributions for laminar flow entrance

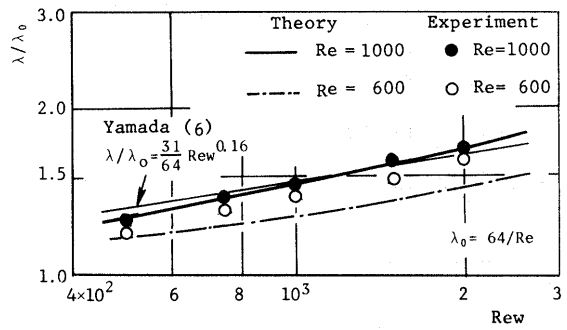

Fig. 12 Relationship between λ/λ_0 and R_{ew} for laminar flow entrance

disturbed by the rotating wall and become ultimately turbulent. Thus, with the use of a turbulent flow analogy, degree of the disturbance is assumed to be decided by a modified mixing length defined by Eq. (32). The axial velocity profiles calculated by this method (when $R_e = 10^3$) are compared with the experimental results in Fig. 11(b), showing a good coincidence. The coincidence, however, becomes a little poor in case of Re = 600, but their tendencies are quite similar. For more advanced calculations, another equation for the mixing length must be used instead of Eq. (32).

Distribution of the tangential velocities in this flow shows a nearly forced vortex type profile ($V/V_0 = r/a$) as is seen in Figs. 11(a) and (b), where a parabolic profile valid for the turbulent flow entrance is also plotted for comparison.

5.2.2 Friction coefficient

Figure 12 shows the relationship between the friction coeffficient λ and the rotational Reynolds number R_{ew} when a laminar flow is introduced. The value of λ is shown dimensionlessly by use of $\lambda_0 = 64/R_e$ available for a stationary pipe. The value of λ/λ_0 increases with R_{ew}, which corresponds to the change in the axial velocity profile. The calculated curve for $R_e = 1000$ agrees well with the experimental results and with a fine solid curve by Yamada's empirical equation.

6. Conclusions

Calculations were made for a flow in the saturated region in an axially rotating pipe by using a modified mixing length theory and the results are compared with experiment. The following are the essentials:

(1) When a turbulent flow is introduced into a rotating pipe, changes in the velocity distribution and friction coefficient due to the tangential velocity given by the rotating wall can be accurately calculated with the value of $\beta = 0.4 \sim 0.5$ in Eq. (15). With an increase in N, the mixing length is decreased and becomes substantially zero when N exceeds 3.5, at which the axial velocity profile changes into a laminar flow type.

(2) Destabilizing effect appears on a flow in a rotating pipe when a laminar flow is introduced into the pipe. Changes in velocity distribution and friction coefficient by this effect can be calculated by use of a modified mixing length, Eq. (32).

Acknowledgement

Authors wish to express their appreciation to Mr. H. Kanda and Mr. H. Murakami of the Hydraulic Laboratory of Nagoya University and also to Mr. T. Ashizaki, Mr. A. Hida and Mr. T. Noguchi for their contributions to the experiment.

References

(1) White, A., J. Mech. Eng. Sci., 6-1 (1964), 47.
(2) Levy, F., Forsch. -h., 322(1929), 18.
(3) Щукин, В. К., Инженерно Физический Журнал, 12-6 (1967), 782.
(4) Murakami, M., et al. Trans. JSME, 42-358(1976), 1784 (in Japanese).
(5) Murakami, M., et al. Trans. JSME, 47-424, B(1981), 2274 (in Japanese).
(6) Yamada, Y., and Imao, S., Trans. JSME, 46-409, B(1980), 1662 (in Japanese).
(7) Koosinlin, M. L., et al., Trans. ASME, Ser. C, 96-2(1974), 204.
(8) Aguilar, F. and Pierce, F. J., Trans. ASME, J. Fluid Eng., 101-2(1979),251.
(9) Launder, B. E., et al., Trans. ASME, Ser. I, 99-1(1977), 231.
(10) Bradshaw, P., J. Fluid Mech., 36-1 (1969), 177.
(11) Pedley, T.LJ., J. Fluid Mech., 35-1 (1969), 97.
(12) Kikuyama, K., et al., Trans. JSME, 48-429, B(1982), 896 (in Japanese).